Journal of Experimental Marine Biology and Ecology 526 (2020) 151335

Contents lists available at ScienceDirect

Journal of Experimental Marine Biology and Ecology

journal homepage: www.elsevier.com/locate/jembe

Skeletal integrity of a marine keystone predator (*Asterias rubens*) threatened by ocean acidification

Sarah Di Giglio[a,*], Etienne Lein[b,c], Marian Y. Hu[d], Meike Stumpp[e], Frank Melzner[b], Loïc Malet[f], Philippe Pernet[a], Philippe Dubois[a]

[a] Laboratoire de Biologie Marine, Université Libre de Bruxelles, 1050 Bruxelles, Belgium
[b] Helmholtz Centre for Ocean Research Kiel (GEOMAR), 24105 Kiel, Germany
[c] Max Planck Institute of Animal Behavior and University of Konstanz, 78464 Konstanz, Germany
[d] Institute of Physiology, Christian- Albrechts-University Kiel, Kiel, Germany
[e] Institute of Zoology, Comparative Immunobiology, Christian-Albrechts- University Kiel, Kiel, Germany
[f] Materials Engineering, Characterization, Synthesis and Recycling (4MAT), Brussels School of Engineering (Faculty of Applied Sciences), Université Libre de Bruxelles, 1050 Bruxelles, Belgium

ARTICLE INFO

Keywords:
Ocean acidification
Echinoderms
Asterias rubens
Skeleton
Mechanics
Acclimation

ABSTRACT

The current increase in atmospheric CO_2 concentration induces changes in the seawater carbonate system resulting in decreased pH and calcium carbonate saturation state, a phenomenon called ocean acidification (OA). OA has long been considered as a major threat to echinoderms because their extensive endoskeleton is made of high-magnesium calcite, one of the most soluble forms of calcium carbonate. Numerous studies addressed this question in sea urchins, but very few questioned the impact of OA on the sea star skeleton, although members of this taxon do not compensate their extracellular pH, contrary to most sea urchins. In the present study, adults of the common sea star, *Asterias rubens* from Kiel Fjord, a site experiencing natural acidification events exceeding pCO_2 levels of 2500 µatm, were chronically exposed to different levels of simulated ocean acidification ($pH_{T\text{-}SW}$ 8.0, 7.4, 7.2), encompassing present and future conditions, for the duration of 109 days. Corrosion and mechanical properties of skeletal elements were studied using scanning electron microscopy, three-point bending tests as well as nanoindentation. The spines were significantly corroded at $pH_{T\text{-}SW}$ 7.4 and below while the ambulacral plates were only affected at $pH_{T\text{-}SW}$ 7.2. Nanoindentation of newly formed spines and ambulacral plates did not reveal significant CO_2-induced differences in skeleton hardness or elasticity across treatments. Results of three-point bending tests revealed significantly reduced characteristic strength and fracture force of ambulacral plates from the median arm segment at $pH_{T\text{-}SW}$ 7.4 and below. These plates are those supporting the tube feet involved in the opening of bivalves during feeding and in the animal attachment to the substrate. Under reduced seawater pH, this might result in fracture of sea star plates during predation on mussel. The present results predict a possible impact of ocean acidification on the skeletal integrity of a marine keystone predator.

1. Introduction

The concentration of atmospheric carbon dioxide (CO_2) has been increasing continuously from the Industrial Revolution onwards, leading to worldwide climatic changes at rates that have never been experienced in the geological past (Caldeira and Wickett, 2003). A part of this CO_2 (~30%) is taken up by the ocean inducing a decrease of pH and alterations in the carbonate chemistry of seawater, a process being known as ocean acidification (OA) (Cao and Caldeira, 2008; Gattuso and Hansson, 2009). Until now, the global ocean surface seawater pH has already decreased by 0.1 pH unit since pre-industrial times. An additional decrease of 0.1–0.3 units - corresponding to seawater pCO_2s 550µatm and 800 µatm - is expected by the end of this century and up to 0.7 pH units (1900 µatm) by the year 2300 (IPCC, 2014). Additionally, the saturation horizon of calcium carbonate is expected to migrate towards the surface (Andersson et al., 2005; Orr et al., 2005).

Abbreviations: OA, Ocean Acidification; pCO_2, partial pressure in CO_2; F_{max}, force at fracture; I_2, second moment of area; L_e, effective length of the plate; h, height of the plate; ΔL, displacement; E, Young modulus; σ, stress; n, number of replicates; S, surface; M, the moment about the neutral axis; y, the perpendicular distance to the neutral axis; I_x, about the neutral axis *x*; ε, the strain; H, Hardness

* Corresponding author at: Avenue F.D. Roosevelt 50, 1050 B-Bruxelles, Belgium.
E-mail address: digiglio.sarah@gmail.com (S. Di Giglio).

https://doi.org/10.1016/j.jembe.2020.151335
Received 16 July 2019; Received in revised form 31 January 2020; Accepted 4 February 2020

Table 1
Seawater chemistry in the three different pH (high, moderate and low pH) treatments during the 109 days experiment (mean ± sd, n = 3).

Treatment	Measured											
	C_T			A_T			Temperature			Salinity		
	($\mu mol\ kg_{SW}^{-1}$)			($\mu mol\ kg_{SW}^{-1}$)			(°C)					
High	2032	±	13	2101	±	8	9.8	±	1.0	15.8	±	0.7
Moderate	2158	±	3	2092	±	9	9.7	±	1.1	15.8	±	0.7
Low	2257	±	18	2103	±	27	9.8	±	1.1	15.8	±	0.7
Treatment	Calculated pCO_2 (µatm)			pH_T			$\Omega_{Calcite}$			$\Omega_{Aragonite}$		
High	489	±	80	8.00	±	0.01	1.83	±	0.25	1.07	±	0.15
Moderate	1867	±	161	7.44	±	0.04	0.53	±	0.05	0.41	±	0.03
Low	3407	±	209	7.19	±	0.03	0.29	±	0.03	0.18	±	0.01

In many seasonally hypoxic coastal habitats, frequent upwelling of CO_2 enriched water leads to higher pCO_2 values and lower pH values than observed in the global ocean. These impact shallow communities dominated by calcifying invertebrates (Thomsen et al., 2013). Kiel Ford is characterized by upwelling of hypoxic (low pO_2 levels) and hypercapnic (high pCO_2 levels) waters that can reach pCO_2s up to *ca.* 800 µatm (seawater pH_T, $pH_{T\text{-}SW}$, 7.8), with peak values exceeding 2500 µatm for several days almost every year ($pH_{T\text{-}SW}$ 7.3) and, in rare instances, 3200 µatm ($pH_{T\text{-}SW}$ 7.2) (Fietzek and Hiebenthal, 2017; Hiebenthal et al., 2016; Melzner et al., 2013; Reusch et al., 2018; Thomsen et al., 2017; Thomsen et al., 2010) pCO_2 levels expected in the Kiel Fjord during the 21st century might reach peak values of 4500 µatm ($pH_{T\text{-}SW}$ 7.1) at an atmospheric pCO_2 double the current one and values ≥3200 µatm ($pH_{T\text{-}SW}$ 7.2) will probably occur at a higher frequency (Melzner et al., 2013). Thus, Kiel Fjord can be used as a natural laboratory to study to what degree calcifying invertebrates can adapt to high CO_2 environments (*e.g.*, Thomsen et al., 2017). OA has direct and indirect adverse effects on physiological processes of marine calcifying organisms, such as growth and biomineralization (Collard et al., 2016; Hu et al., 2018b; Kroeker et al., 2013; Melzner et al., 2009; Wittmann and Pörtner, 2013). Indeed, increased seawater proton concentration ($[H^+]$) raises the energetic cost to remove protons produced during $CaCO_3$ skeletons formation (Cyronak et al., 2015; Suwa et al., 2014) and a decreased $CaCO_3$ saturation state may induce dissolution of skeletons that are not sufficiently protected by organic structures (Dery et al., 2017; Naviaux et al., 2019).

Sea stars are considered as keystone predators in several ecosystems, controlling mollusc populations, particularly bivalves (Navarrete and Menge, 1996; Paine, 1974; Saier, 2001; Uthicke et al., 2009). Forcipulatid sea stars (like *Asterias* and *Pisaster*), a taxon of predator species, are able to open bivalve shells by pulling with tube feet and arms on the valves (Norberg and Tedengren, 1995) inducing a narrow opening of the valves, followed by the extraoral digestion of the bivalve tissues through the evaginated stomach (Anger et al., 1977; Mcclintock and Robnett, 1986). This opening of the valves is carried out by the tube feet supported through the skeletal plates, which bear the maximum stress during this process (Eylers, 1976). The same is true when the sea star has to withstand hydrodynamical forces generated by wave exposure (Flammang, 1996). Therefore, the skeleton is crucial for 'mechanical autoecology' and any compromising effects of OA on this structural integrity might have far ranging consequences for the ecological fitness of sea stars.

The sea star skeleton is made of high magnesium-calcite (Chave, 1954; Weber, 1969). Depending on its magnesium concentration, this material is one of the most soluble forms of calcium carbonate and, under abiotic conditions, more susceptible to dissolution compared to skeletons formed only of calcite or aragonite (Lebrato et al., 2016; Morse et al., 2006). To the best of our knowledge, to date, no study has investigated the impact of OA on corrosion or mechanical properties of the skeleton in sea stars (Byrne and Fitzer, 2019). Furthermore, conflicting results were reported about OA effects on sea star growth rate, which can serve as a possible indirect indicator of skeleton stability (Table S1). At comparable level and duration of exposure, some studies reported a significantly decreased growth rate in *A. rubens* (Appelhans et al., 2012, 2014; Hu et al., 2018; Keppel et al., 2015) while others measured no significant effect or an increased growth rate in *Pisaster ochraceus*, *Acanthaster planci* or *Luidia clathrata* (Gooding et al., 2009; Kamya et al., 2017; Kamya et al., 2016; Schram et al., 2011). The same individuals *A. rubens* used in the present study had significantly reduced growth and feeding rates at low $pH_{T\text{-}SW}$ (7.4 and 7.2) after 85 and 105 days of exposure (Hu et al., 2018). This suggests that, at these low pH, either the skeleton of the sea stars could be affected by OA or that the skeleton properties could be maintained at the expense of growth.

Therefore, the goal of the present study was to assess the effects of several levels of OA on the skeleton of the North Atlantic keystone predator sea star *Asterias rubens* (Linnaeus, 1758) during a 109 days CO_2/pH perturbation experiment. Corrosion of different ossicles was assessed and nanoindentation and three-point bending tests were carried out.

2. Materials and methods

2.1. Seawater acidification experiments

All samples came from the adult sea stars *Asterias rubens* analysed in Hu et al. (2018). Briefly, these were collected in Kiel Fjord, which is characterized by upwelling of hypoxic and hypercapnic waters (see Introduction). Sea stars were exposed to three different treatments for 109 days: high pH (control, pH_T 8.0, pCO_2 = 489 µatm), moderate pH (current values during upwelling episodes, pH_T 7.4, pCO_2 = 1867 µatm), and low pH (current unfrequent extreme values whose frequency is expected to increase during the 21st century, pH_T 7.2, pCO_2 = 3407 µatm) (Table 1). pH in the experimental tanks was controlled by a central automatic CO_2 mixing unit ($KICO_2$ – Kiel CO_2 manipulation experimental facility, Linde Gas & HTK Hamburg, Germany) that supplied air continually containing the appropriate pCO_2 partial pressures. Ten independent tanks per condition hosted five sea stars of each size range, only one per tank was used for the present study. During the experimental period, tanks were connected to a water flow-through system, constantly supplying animals with fresh seawater from Kiel Fjord at a rate of 66–100 ml min^{-1}. Flow rates of gas and water were adjusted in such a way as to enable full equilibration of the tank water with the respective gas mixture. Sea stars were fed *ad libitum* with mussels (*Mytilus edulis*) of appropriate size collected in the Kiel Fjord (Hu et al., 2018).

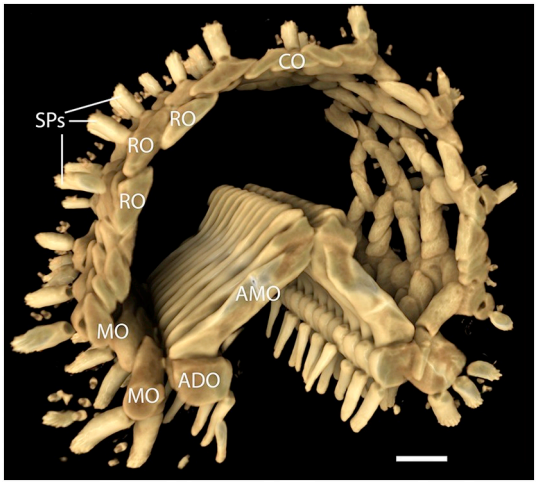

Fig. 1. X-ray microtomography of the ray endoskeleton of *Asterias rubens*, Ad SPs: adambulacral spines, ADO: adambulacral plate, AMO: ambulacral plate, CO: carinal ossicle, MO: marginal ossicle, RO: aboral ossicle and Sub SPs: subambulacral spines. Figure from Blowes et al., 2017.

2.2. Preparation of ambulacral plates and spines

At the end of the experiment, five to seven sea stars (each from a different tank from each treatment, arm size range: 68–144 mm) were collected from the different treatments, inner organs were removed and the integument air-dried completely for 48 h at 25 °C. One to four arms per sea star (Table S2) were dissected for mechanical tests. On each arm, ambulacral plates and ad- and sub-ambulacral spines (Fig. 1.) from three segments of the arms were sampled: distal (= tip of the arm), median and proximal (= closest to the central disc). In sea star, new ossicles are formed at the proximal margin of the terminal plates, which is located at the tip of the arm (Fewkes, 1888; Hotchkiss, 2012). Consequently, plates closest to the central disc are the oldest ones and those closest to the arm tip are the youngest ones. Because sea star in all treatments effectively grew (Hu et al., 2018), plates in median position at the end of the experiment were in distal position at the beginning. This also means that these plates increased in size during the experiment so that a part of each plate was deposited before the experiment and a part during this. The ossicles were cleaned of soft tissues by soaking the segments in NaOCl 2.5% for 60 min. followed by NaOCl 5.25% for 90 min. and rinsed with MilliQ water between the two soaking steps. The skeletal parts were air-dried for 12 h before further analysis.

2.3. Scanning electron microscopy (SEM)

SEM analyses were carried out on three ambulacral plates, three subambulacral spines and three adambulacral spines of each segment per arm per individual (5 to 8) and per treatment. All cleaned plates and spines were mounted on aluminum stubs, coated with gold (JEOL JFC-1100E) and images were acquired with a JEOL JSM-7200F scanning electron microscope. Corrosion was quantitatively assessed as:

$$corrosion = \frac{number\ of\ corroded\ ossicles}{total\ number\ of\ analysed\ ossicles}$$

Two types of corrosion were recognized in SEM. Type 1 was superficial and consisted of tiny holes (0.16 to 0.64 μm) or weathering of the superficial layer of the stereom (Fig. 2 A + B) while type 2 resulted in deep grooves (large of 0.31 to 0.77 μm) and pits (Fig. 2. C).

2.4. Mechanical tests

2.4.1. Three-point bending test

All mechanical tests were performed on the individual plates, due to their very small size, spines were not tested. Mechanical tests were carried out at room temperature (18 to 20 °C). To measure the fracture force of the ambulacral plates, a three-point bending test was carried out according to Moureaux et al. (2011). The largest (*i.e.,* the oldest) plates in the proximal segment, the medium sized plates from the median segment, and the smallest (*i.e.,* the youngest) plates from the distal segment were analysed. Each ambulacral plate was first photographed sideways in front of graph paper to measure the effective length (length between the two supporting points), using ImageJ software (Rasband,W.S., U.S.National Institutes of Health, Bethesda,MD, USA). They were then placed on a homemade metal stand and the mechanical test was performed using a non-cutting blade fixed on the load frame of the force stand (Instron 5543), which was lowered on the middle of the plate at a speed of 0.1 mm min^{-1} until fracture. Displacement and force were recorded continuously at a frequency of 10 Hz. One of the two halves of the plates were recovered after fracture and one was mounted on an aluminum stub, coated with gold for 2 min (JFC-1100 E ion sputter), and observed in a scanning electron microscope (JEOL JSM-7200). Digital pictures of the cross sections were recorded and subsequently examined in ImageJ with the macro Moment Macro developed for the calculation of the second moment of area (I_2) (Ruff C., Johns Hopkins University School of Medicine, MD, USA). I_2 is a description of the geometric distribution of material around a neutral axis of bending and reflects the proportion of stereom in the plate fracture surface (*vs.* pores).

$$I_2 = \int y^2\, dA\ (m^4)$$

The apparent Young modulus (E), characterizing the material stiffness, was calculated according to the linear-elastic beam theory:

$$E = \frac{stress}{strain} = \frac{\sigma}{\varepsilon} = \frac{F/A}{\Delta L/L}\ (Pa)$$

$$E = \frac{F_{max}\, L_e^3}{48\, \Delta L I_2}\ (Pa)$$

where F: force (N), F_{max}: force at fracture (N), A: area (in transverse section) (m^2), ΔL: displacement (m), L = L_e: effective length (m), I_2: second moment of inertia (m^4) (Moureaux et al., 2011).

Flexural stress of the ossicle in a beam under three-point bending was calculated following the classic formula of Euler–Bernoulli beam theory:

$$\sigma = -\frac{M}{I_x} y = E.\ \varepsilon = \frac{F_{max}\, L_e^2}{48\, I_2} (\mathrm{Pa})$$

where σ: the bending stress at fracture (Pa), M: the moment about the neutral axis (Nm), y: the perpendicular distance to the neutral axis (m), I_x about the neutral axis x (m^4) and ε, the strain (=ΔL/L, dimensionless).

2.4.2. Nanoindentation

For nanoindentation analysis, three adambulacral spines and three ambulacral plates from the distal segment of the arm, (the youngest part of which consisting of calcite that has only been deposited during the experiment, based on the sizes of the sea stars at the beginning and at the end of the experiments) from five individuals were analysed for each treatment. They were embedded in epoxy resin (Struers ®, Gmbh), then ultra-polished using sandpapers of decreasing grain size (from P180 (82 μm) to P4000 (5 μm), FEPA Struers®) and aluminum oxide (3 μm to 1 μm) until the calcium carbonate of the skeleton was exposed to the surface and properly polished. The obtained sections were perpendicular to the growth axis. Four to eight useful indents were

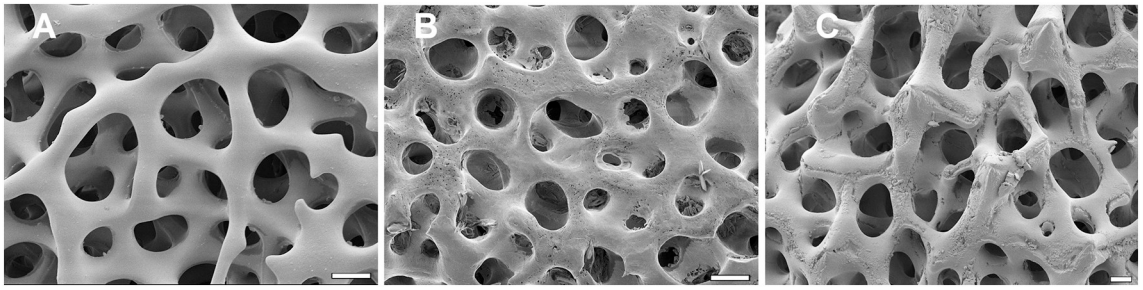

Fig. 2. Scanning electron micrographs showing the different types of corrosion observed in the stereom of ossicles of *Asterias rubens*. A: no corrosion, B: corrosion type 1, C: corrosion type 2. Scale bar = 10 μm.

obtained in the cross section of each ossicle by a nanoindenter (TriboIndenter, Hysitron, Minneapolis, MN, USA) with a charge of 3000 μN using a Berkovich tip (a low charge was chosen to avoid any confounding effect of the resin; Presser et al., 2010). Young modulus (E) and hardness (H) values of the calcite were determined from the unloading curve of the indentation test (Oliver and Pharr, 1992).

2.5. Sample preparation and analysis of magnesium content

Samples (containing between 1.2 and 6.9 mg of powdered skeleton from distal and proximal segments) were mineralized in a Milestone 1200 M microwave oven in 2.5 ml HNO_3 (65%) and 1 ml H_2O_2 (30%). The resulting solution was filtered on a GF/A Whatman filter and brought to a final volume of 25 ml with ultrapure water (Sartorius). The solutions were diluted 10 times in acidified water (HNO_3 SupraPur 5%) prior to analyses. Mg concentration of the solutions was analysed with a flame atomic absorption spectrometer (GBC 906 AA). The calibration was achieved using artificial multi-elemental solutions made from certified mono-elemental solutions (Merck) and quality control was carried out using certified reference material (1.51 g/kg Mg, Govindaraju, 1994; Moureaux et al., 2011). Results for the certified reference materials were within ± 7.2% of the certified values (1.53 ± 0.05 g/kg Mg, n = 13).

2.6. Statistical analysis

For ANOVA statistical analysis, appropriate multiple comparison tests (Tukey tests following ANOVA) were carried out following Doncaster and Davey (2007) instructions. Proportions of corroded ossicles were transformed as arcsine square root transformed and analysed by ANOVAs model III (treatment: fixed factor, individual: random factor nested in treatment, segment of the arm: crossed repeated fixed factor) for two types of corrosions and for each type of ossicle. Young modulus (E) and hardness (H) obtained by nanoindentation were analysed using model III ANOVA (treatment: fixed factor, individual: random factor nested in treatment, plate: random factor nested in individual). Results of Mg concentration were analysed using model III ANOVA (treatment: fixed factor, individual: random factor nested in treatment, segment: crossed repeated fixed factor). For mechanical properties of ambulacral plates, F_{max}, I_2, Young modulus (E), stress (σ) and L_e, were compared to the respective treatment using model III ANOVAs (treatment: fixed factor, individual: random factor nested in treatment, segment of the arm: crossed repeated fixed factor) followed by Tukey test. Then, mechanical properties (F_{max}, Young modulus (E) and stress (σ),) of all plates from of each pH treatment and segment were further analysed using Weibull distribution, a method to characterize failure of brittle materials. Weibull probabilistic statistics applied to mechanical properties of ambulacral plates of *Asterias rubens* are presented in Supplementary Information (S1).

3. Results

3.1. Corrosion

In ambulacral plates, corrosion Type 1 was recorded in all arm segments, almost exclusively at pH 7.2. The proportion of affected plates in distal and proximal segments was significantly higher at pH 7.2 compared to the two other treatments (Table 2). Corrosion Type 1 was recorded in all treatments and all segments in adambulacral and subambulacral spines, but the proportion of occurrence was significantly higher at pH 7.2 compared to the two other treatments. Corrosion Type 2 was only recorded in ambulacral plates from the distal (youngest) arm segment exposed to seawater at pH 7.2, but the proportion of affected ossicles was not significantly different from that recorded in the two other treatments. Besides, corrosion Type 2 occurred at pH 7.4 and 7.2 but its proportion of occurrence was only significantly higher at pH 7.2, compared to the two other treatments (Table 2). The interaction terms between arm segment and pH were never significant ($p_{ANOVA} \geq 0.089$, Table S3). The segment had a marginally significant effect ($p_{ANOVA} = 0.048$) for corrosion Type 2 in subambulacral spines (Table S3).

3.2. Mechanical properties of ambulacral plates

When tested by ANOVA, pH and the interaction between pH and the arm segment had no significant effect on mechanical and morphometrical properties ($p_{ANOVA} \geq 0.092$ and $p_{ANOVA} \geq 0.104$, respectively) (Table S5). On the contrary, all mechanical and morphometrical properties significantly differed according to the arm segment ($p_{ANOVA} \leq 0.028$) (Table 3 and Table S5).

Dispersion of values in mechanical tests as observed here (Table S4) is a frequent feature. Therefore, a Weibull analysis of the results was carried out. The Weibull modulus for stress in ambulacral plates ranged between 0.808 and 1.417. It significantly differed according to the considered arm segment, being higher in the median and distal segments than in the proximal segment at pH 8.0 (Fig. 3, Table 4). At pH 7.4, it was significantly higher in distal plates than in median and proximal plates. At pH 7.2, Weibull modulus was significantly higher in the median segment than in other segments ($p_{ANCOVA} < 10^{-3}$, Table S6). It also significantly differed in different pH treatments ($p_{ANCOVA} < 10^{-3}$). In distal plates, it was significantly lower at pH 7.2 than at pH 8.0 and 7.4 ($p_{Tukey} < 10^{-3}$). On the contrary, in median plates, it was significantly lower at pH 8.0 than at pH 7.4 and 7.2 ($p_{Tukey} < 10^{-3}$), and in proximal plates, it was significantly higher at pH 7.2 ($p_{Tukey} < 10^{-3}$) (Fig. 3, Table S7.1).

The characteristic strength (σ_0) is a reference measure in the field of mechanics. It is the stress (F_{max}/Surface) required to break 63.2% of the samples. Based on the respective 95% confidence intervals, the characteristic strengths only differed significantly in median ambulacral plates, being higher at pH 8.0 than at pH 7.4 and 7.2 (Fig. 3, Table 4, Table S7.1).

Table 2
Quantitative measures of corrosion on ambulacral plates and ad- and subambulacral spines on different segments of *A. rubens* arms (distal, median and proximal) undere three different pH conditions (mean ± sd, $n = 5$) and results of ANOVA and Tukey tests for factor pH per arm segment (means sharing the same superscript are not significantly different, NT: no test).

Ambulacral plates											
	$pH_{T\text{-}SW}$	8.0			7.4			7.2			p_{ANOVA}
		n = 5			$n = 8$			$n = 7$			
Corrosion 1	Distal	0% ^{b}	±	0%	10% ^{a,b}	±	23%	36% ^{a}	±	30%	**0.011**
	Median	0%	±	0%	0%	±	0%	10%	±	19%	0.172
	Proximal	0% ^{b}	±	0%	0% ^{b}	±	0%	26% ^{a}	±	16%	**$< 10^{-3}$**
Corrosion 2	Distal	0%	±	0%	0%	±	0%	11%	±	16%	0.140
	Median	0%	±	0%	0%	±	0%	0%	±	0%	NT
	Proximal	0%	±	0%	0%	±	0%	0%	±	0%	NT
Adambulacral spines											
	$pH_{T\text{-}SW}$	8.0			7.4			7.2			p_{ANOVA}
		n = 5			n = 8			n = 7			
Corrosion 1	Distal	3%	±	7%	27%	±	32%	31%	±	15%	0.117
	Median	0% ^{b}	±	0%	8% ^{b}	±	18%	33% ^{a}	±	24%	**0.012**
	Proximal	3% ^{b}	±	7%	15% ^{b}	±	23%	55% ^{a}	±	26%	**0.001**
Corrosion 2	Distal	0% ^{b}	±	0%	2% ^{b}	±	6%	25% ^{a}	±	21%	**0.001**
	Median	0% ^{b}	±	0%	0% ^{b}	±	0%	31% ^{a}	±	21%	**0.001**
	Proximal	0% ^{b}	±	0%	0% ^{b}	±	0%	14% ^{a}	±	16%	**0.012**
Subambulacral spines											
	$pH_{T\text{-}SW}$	8.0			7.4			7.2			p_{ANOVA}
		n = 5			n = 8			n = 7			
Corrosion 1	Distal	0% ^{b}	±	0%	23% ^{b}	±	25%	62% ^{a}	±	23%	**$< 10^{-3}$**
	Median	7% ^{b}	±	15%	23% ^{b}	±	34%	74% ^{a}	±	23%	**0.001**
	Proximal	0% ^{b}	±	0%	10% ^{b}	±	20%	62% ^{a}	±	28%	**$< 10^{-3}$**
Corrosion 2	Distal	0% ^{b}	±	0%	6% ^{a,b}	±	12%	25% ^{a}	±	21%	**0.003**
	Median	0% ^{b}	±	0%	0% ^{b}	±	0%	11% ^{a}	±	13%	**0.040**
	Proximal	0% ^{b}	±	0%	0% ^{b}	±	0%	12% ^{a}	±	13%	**0.039**

The force needed to break 63.2% of the plates (F_{max0}, Fig. 4, Table 5, Table S7.2,) only differed in median plates, being significantly higher at pH 8.0 than at pH 7.2. At pH 8.0 and 7.4, F_{max} was significantly lower in distal plates than in median and proximal plates. At pH 7.2, it was significantly lower in distal plates than in proximal plates but not in median plates.

Young modulus of 63.2% of the ambulacral plates (E_0, Table 6, Table S7.3) did not differ according to the treatment. At pH 8.0, E was significantly higher in distal plates than in proximal plates but not median plates. At pH 7.4, E was significantly higher in distal plates than in median plates and proximal plates. At pH 7.2, E was not significantly different according to the segment.

3.3. Nanoindentation

pH did not affect the nanohardness and nanoelasticity of either distal adambulacral spines or distal ambulacral plates ($p_{ANOVA} \geq 0.063$) (Table 7, Table S8).

3.4. Magnesium content of the skeleton

There were no significant differences between the pH in terms of $MgCO_3$ concentration in the skeleton ($p_{ANOVA} = 0.909$). However, $MgCO_3$ concentration was significantly higher in distal than in proximal plates ($p_{ANOVA} = 0.040$, Table 8, Table S9).

4. Discussion

Mechanical stability of ossicles is critical for the diverse functions of the echinoderm skeleton including movements of the animal, feeding activity and attachment to substrate. In the present study, we recorded both dissolution (corrosion) and changes in important mechanical properties of the skeletal parts of *Asterias rubens* exposed to seawater acidification during a 109 days period.

4.1. Corrosion

Corrosion was observed in both, ambulacral plates and spines. It was equal or close to 0% in control sea stars, indicating that corrosion

Table 3
Mechanical and morphometrical properties of ambulacral plates of *A. rubens* according to segments (pooled treatment, mean ± sd, $n = 20$) and results of ANOVA and Tukey tests for factor segment. (means sharing the same superscript are not significantly different).

Segment of the arm	Distal			Median			Proximal			$p_{ANOVA\ segment}$
	n = 20			n = 20			n = 20			
F_{max} (N)	0.49^{b}	±	0.10	0.73^{a,b}	±	0.31	1.11^{a}	±	0.47	$< 10^{-3}$
E (Gpa)	13.90^{a}	±	12.48	5.93^{a,b}	±	3.67	3.70^{b}	±	2.18	$< 10^{-3}$
Stress (MPa)	89.46^{a}	±	52.03	50.79^{a,b}	±	25.14	44.82^{b}	±	23.91	0.028
ΔL (mm)	0.027^{b}	±	0.012	0.043^{a,b}	±	0.015	0.061^{a}	±	0.023	$< 10^{-3}$
Height (mm)	0.30^{b}	±	0.02	0.42^{a,b}	±	0.08	0.50^{a}	±	0.10	$< 10^{-3}$
I_2 (10^9 μm^4)	2.47^{b}	±	3.22	4.61^{a,b}	±	1.41	16.48^{a}	±	10.85	$< 10^{-3}$
L_e (mm)	2.19^{b}	±	0.35	3.19^{a,b}	±	0.35	3.81^{a}	±	0.86	$< 10^{-3}$

F_{max}, force at fracture (N); I_2: second moment of area (μm^4); L_e: effective length of the plate (mm); h: height of the plate (mm), ΔL: displacement (mm); E, Young modulus calculated from the mechanical test (three-points bending) (GPa); σ: stress calculated from Euler-Bernouilli formula (MPa); n: number of replicates.

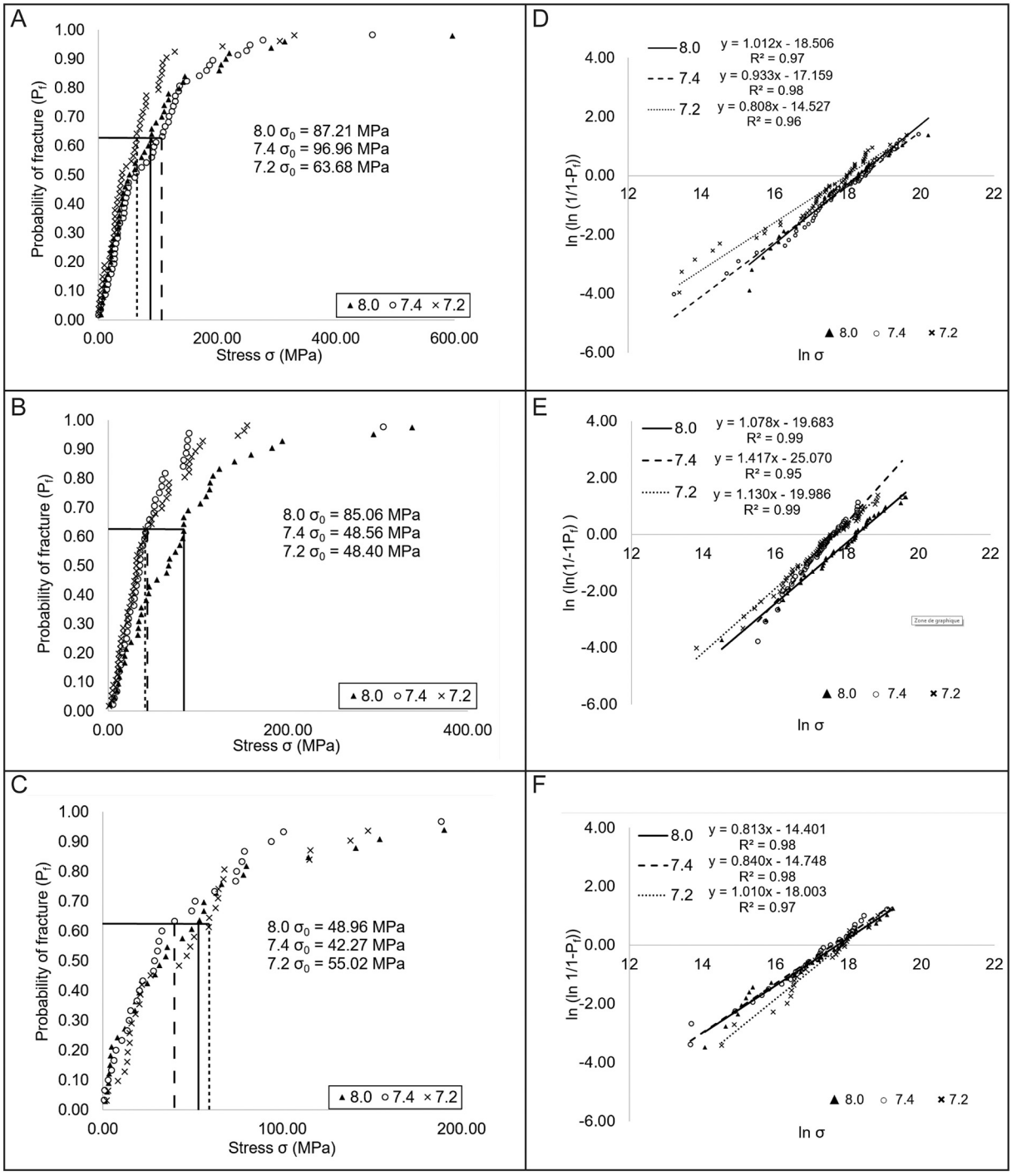

Fig. 3. Weibull plots and linearized curves of fracture stress from ambulacral plates of distal (A, D), median (B,E) and proximal (C, F) segments of the arm of adult sea star *A. rubens* submitted to the three treatments (pH 8.0, 7.4, 7.2).

recorded at low pH was not a bleaching artefact. Its occurrence was significantly higher at pH 7.2 and spines were more seriously impacted than ambulacral plates. This was also reported for sea urchins where spines were found to be more corroded than the test plates (Dery et al., 2017 and references therein). This was attributed to the much thinner tissue layers covering the spine skeleton (Dery et al., 2017). However, in sea urchins, test plates were almost completely devoid of corrosion while *A. rubens* ambulacral plates were negatively impacted. Holtmann et al. (2013) reported that the mesothelium covering the sea urchin test plates on their inner side is permeable to bicarbonate. However, even when the coelomic fluid (the main extracellular fluid compartment) is under-saturated with respect to calcium carbonate, test plates are not corroded, suggesting that test plates are efficiently protected (Dery et al., 2017). On the other hand, most sea urchins partly compensate their extracellular pH (pH_e) when facing hypercapnic conditions (high pCO_2 level) while *Asterias rubens* does not (Appelhans et al., 2012; Collard et al., 2013; Stumpp et al., 2012). However, cidaroids, a basal group of sea urchins do not compensate their pH_e and have naturally very low pH_e ($pH_T \leq 7.0$) (Collard et al., 2015; Collard et al., 2014). Despite this, their test plates also show no trace of corrosion even under decreased seawater pH of 7.2 (Dery et al., 2017). Therefore, a possible absence of pH_e compensation cannot *per se* be attributed as the cause of

Table 4
Results of Weibull model applied to stress (σ).

Segment of the arm	Distal								Median						Proximal							
Nominal pH	n	m		C		R^2	σ_0 (MPa)	σ_0 (MPa) $IC_{95\%}$ -	σ_0 (MPa) $IC_{95\%}$ +	n	m		C	R^2	σ_0 (MPa)	σ_0 (MPa) $IC_{95\%}$ -	σ_0 (MPa) $IC_{95\%}$ +	n	m		C	R^2	σ_0 (MPa)	σ_0 (MPa) $IC_{95\%}$ -	σ_0 (MPa) $IC_{95\%}$ +
8.0	49	1.012	a	−18.506	0.973	87.21	a	64.67	117.60	41	1.078	b	−19.683	0.988	85.06	a	62.61	115.66	32	0.813	b	−14.401	0.977	48.96	a	30.88	77.55
7.4	56	0.933	a	−17.159	0.976	96.96	a	71.59	131.32	43	1.417	a	−25.0697	0.951	48.56	b	38.67	61.02	29	0.840	b	−14.748	0.981	42.27	a	26.46	67.51
7.2	52	0.808	b	−14.527	0.960	63.68	a	44.28	91.58	55	1.130	a	−19.986	0.990	48.40	b	37.57	62.29	30	1.010	a	−18.003	0.968	55.02	a	37.53	80.72

m: Weibull modulus (slope of the linearized Weibull curve), C: intercept with y axis, R^2: determination coefficient of linearized data regressions, σ_0: characteristic strength (value at which 63.2% of the plates break), σ_0 IC $_{95\%}$ ±: lower and upper limits of 95% confidence interval. Values sharing the same superscript in the same arm segment for the same variable did not differ significantly.

plate corrosion in *A. rubens*. It should be noticed that metabolic rates of sea star are usually higher than those determined for sea urchins (Hughes et al., 2011) accompanied with higher growth rates of the skeleton (Barnes and Powell, 1951; Guillou et al., 2012). According to this reasoning, this means that sea stars would have a relative surplus of metabolic CO_2 as well as a higher rate of protons release from the precipitation of $CaCO_3$ during skeleton formation. This might result in lower tissue pH than in cidaroids when facing OA, inducing corrosion of the skeleton. Interestingly, young distal ambulacral plates suffered more from corrosion than older proximal plates. This could be due to the intense calcification occurring in distal plates (and the resulting proton production) while proximal plates almost do not grow anymore (Ben Khadra et al., 2015; Hotchkiss, 2012). Alternatively, a higher susceptibility to corrosion in distal plates could be due to the presence of amorphous calcium carbonate in newly formed ossicles, a polymorph of calcium carbonate thirty times more soluble than calcite (Politi et al., 2004).The higher magnesium concentration recorded in distal plates might also be involved in a higher solubility of these plates. However, the difference between distal and proximal plates, although significant, is rather low (*ca.* 1 mol%) and occurs in a range where solubility does not change much with Mg concentration (see Lebrato et al., 2016).

4.2. Mechanical properties

Asterias rubens is a Forcipulatid sea star, a taxon of predator species, which are able to open bivalve shells by pulling with tube feet and forcing a narrow gap between the valves (Norberg and Tedengren, 1995). As *Asterias rubens* uses extraoral feeding whereby the cardiac stomach is extruded and inserted between the valves of the prey, the force needed to open the prey is of major importance (Zafiriou et al., 1972). This force depends on the holding force of the mussel adductor muscles but not on the opening amplitude (Norberg and Tedengren, 1995). Forces acting on sea star ambulacral plates, the main ossicles on the oral face of the sea star ray involved during this process, were studied, at the critical moment of mussel opening, by Eylers (1976) in the closely related *Asterias forbesii.* Forces generated by tube feet activity, nearby plates and muscles were shown to be transferred to the ambulacral arch and concentrated at the insertion of the inferior transverse ambulacral muscle (ITAM), the point where force was applied to the ossicle during the three-point bending tests carried out within this study. Forces are only secondarily transferred to the rest of the body wall (Eylers, 1976). Therefore, force at fracture, elasticity and second moment of inertia of ambulacral plates gave an insight of the impact of OA on the most important part of the forcpulatid skeleton.

No significant effects of OA on mechanical properties of ambulacral plates were detected by ANOVA analysis, which is consistent with previous results on sea urchins test plates (Asnaghi et al., 2019; Collard et al., 2016; Moulin et al., 2015). It is worth recalling that sea star ambulacral plates were significantly corroded while sea urchin plates were not. As usual, mechanical data showed a large range of dispersion, making ANOVA analyses low power statistical tests. The Weibull analysis is frequently used in the field of material research and has been applied here for the first time in the context of global change impact on skeletal material. It revealed that the Weibull modulus for stress was impacted by treatment and arm segment. In newly formed distal plates, it decreased with pH, being significantly lower at pH 7.2. This means that the flaw distribution became more heterogeneous at low pH. This was not paralleled by nanoindentation results in distal plates, which did not differ with treatment, suggesting that the flaw spatial scale differs from that of this technique. On the contrary, in proximal plates, Weibull modulus increased with lower pH meaning that hypercapnic conditions enhanced a less heterogeneous dispersion of flaws within the oldest ossicles. However, for both segments, this was not reflected either in the characteristic strength (σ_0), breaking force (F_{max0}) or in Young modulus (E_0). A lack of relationship between flaw distribution (m) and characteristic strength (σ_0) is not unusual (see *e.g.,* Lin et al., 2006) and

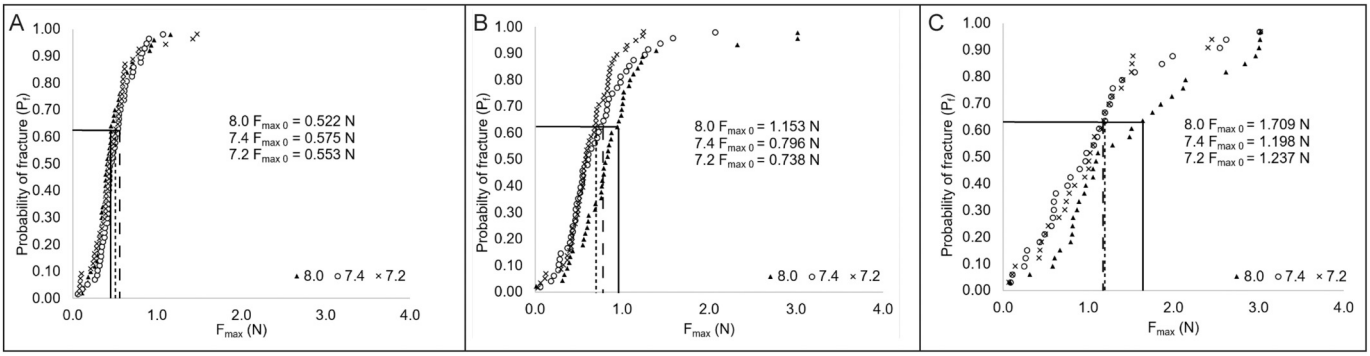

Fig. 4. Weibull plots of F_{max} from ambulacral plates of different segments of the arm (A: distal, B: Median, C: Proximal) of sea star to the treatments (pH 8.0, 7.4, 7.2).

might result from differences in the crack propagation processes (Leung et al., 2015). In control conditions, the Weibull modulus of ambulacral plates was larger in distal than in proximal plates. Accordingly, the youngest plates showed more homogeneous dispersion of flaws than older plates. Similarly, Aizenberg et al. (1997) reported a more anisotropic dispersion of flaws in mature sea urchin spines, compared to young ones. Thus, maturation of the echinoderm skeleton appears to go along with an increase in heterogeneity. Furthermore, in all treatments, proximal ambulacral plates resisted less stress but supported a higher force at fracture and were more elastic than their equivalents in other segments of the arms. Besides the Weibull modulus, distal plates that were formed during the experiment appeared mainly unaffected by the treatment, contrary to the median plates whose characteristic strength was significantly decreased by a factor of two at pH 7.4 and 7.2. These plates were partly formed during the experiment but their core was deposited before the treatment started. If the newly deposited material was affected by the treatment, this could induce a weakness between the original and new material favouring crack propagation.

The present results underline the utility of the Weibull analysis, as it allowed revealing effects that otherwise would have remained undetected with a mixed model ANOVA analysis. However, it should be emphasized that the Weibull analysis requests a minimum of 30 samples per condition (Bütikofer et al., 2015), which implies a rather heavy workload with an increasing number of treatments.

4.3. Biomechanical and ecological impacts

Forces acting during the activity of tube feet while moving or feeding are first transmitted to the ambulacral plates (see 4.2., Eylers, 1976). Information about the actual traction of the tube foot on the ambulacral plates and the maximal stress points where the energy is concentrated on the plates during those movements is scarce in the literature. Norberg and Tedengren (1995) measured a maximal force of 63 N exerted by adult *A. rubens* to open a mussel commensurate with old measures by Paine (1926; 5000 grams *i.e. ca.* 50 N). Mostly podia located in the middle of the arm are used for this activity (Hennebert et al., 2010). The force exerted by each tube foot is principally due to the force exerted by the retractor muscle that Hennebert et al. (2010) measured as ~0.04 N. The detachment force of the tube foot (due to disk adhesion to the substrate and which is lower than the tube foot stem breaking force) is ~0.15 N (recalculated from data provided in Hennebert et al., 2010 for sea stars of similar size than those used in the present study). So, the force exerted by the tube foot on the ambulacral plate is in between these two values. The proportions of plates broken for each force according to pH are presented in Table S10. Two to four times more median plates of animals acclimated to low pH would break in comparison to plates of animals acclimated to intermediate and control pH. If maximally 63 N are needed to open a mussel, this means that the action of in between 1575 (63/0.04) and 420 (63/0.15) tube feet is needed. If all of these were located in the median segment, then 13 (1575 × 0.008) to 29 (420 × 0.069) plates (3 to 6 plates per arm) would break at pH 7.2 (worst-case scenario). Even at pH 7.4, if this was to occur every time a sea star consumes a mussel (about once a day – once a week), this could be a serious impact of OA. Sea stars have high regeneration abilities and are able to heal ossicle fractures (Moureaux et al., 2011) but this would come at substantial energetic costs. Hu et al. (2018) showed that under OA, the same sea stars had a reduced food intake resulting in reduced growth rate and, consequently, diminished energy uptake. This could be linked to the damages caused to the ambulacral plates, reducing the ability of sea stars to open mussels. Combined with the impact of OA on larvae (Hu et al., 2018), this could imperil future sea star populations. *A. rubens* of Kiel Fjord encounters low pH (pH_T 7.3) for several days almost every year and could – therefore – be pre-adapted to acidified conditions (see Thomsen et al., 2017). However, both growth rate and skeletal properties were found to be already affected at pH_T 7.4 (Appelhans et al., 2012, 2014, Hu et al., 2018, present study), indicating that sea star populations from naturally fluctuating habitats might not be particularly resistant to OA and could, on the contrary, already experience conditions close to their upper tolerance limits (Hu et al., 2018). The skeletal integrity of adult *A. rubens* from Kiel Fjord was negatively affected by simulated OA, in particular when the pCO_2 levels slightly exceeded the naturally experienced hypercapnic peaks of the Kiel Fjord. In this high-CO_2 coastal zones, pCO_2 will very probably, in the future, equal those in our low pH treatment for significant periods of time and peak values will exceed these (up to 4500 μatm for a doubled atmospheric pCO_2, pH_T 7.1) (Melzner et al., 2013; Thomsen et al., 2010). However, in the present study, the sea stars were submitted to continuously low pH for almost four months, which would likely exacerbate the effects of OA compared to transient low pH episodes expected in the future. Nevertheless, taken together, our results suggest that sea star populations from this environment could effectively suffer from OA towards the end of the 21st century.

The sea star favoured preys items in Kiel Fjord, the mussel species *Mytilus edulis*, on the contrary, were suggested to have a potential to adapt to hypercapnic conditions (Thomsen et al., 2017). So weaker sea stars will face possibly adapted mussels, further increasing the negative impact of OA on the sea star population. This may probably cascade on the whole community due to the structure role of predator sea stars (Paine, 1974).

5. Conclusions

In the present study, the skeleton of adult *Asterias rubens* from Kiel Fjord was corroded and showed signs of deteriorated mechanical properties when exposed to reduced pH seawater, even at values close to those occasionally encountered in their natural habitat, potentially indicating a limited scope for future adaptation or acclimation and future poor resilience of this population. The skeleton of this sea star species was more affected by OA than that of sea urchins, which is possibly due to a higher metabolism and calcification rate.

Table 5
Results of Weibull model applied to force at fracture (F_{max}).

Segment of the arm	Distal								Median								Proximal							
Nominal pH	n	m	C	R^2	F_{max0} (N)		F_{max0} (N) $IC_{95\%}$ -	F_{max0} (N) $IC_{95\%}$ +	n	m	C	R^2	F_{max0} (N)		F_{max0} (N) $IC_{95\%}$ -	F_{max0} (N) $IC_{95\%}$ +	n	m	C	R^2	F_{max0} (N)		F_{max0} (N) $IC_{95\%}$ -	F_{max0} (N) $IC_{95\%}$ +
8.0	59	2.416	1.569	0.982	0.522	a	0.462	0.593	43	1.295	−0.184	0.998	1.153	a	0.901	1.475	32	1.478	−0.792	0.988	1.709	a	1.326	2.201
7.4	56	2.312	1.280	0.999	0.575	a	0.509	0.650	47	1.824	0.415	0.991	0.796	a,b	0.672	0.943	32	1.338	−0.242	0.983	1.198	a	0.906	1.585
7.2	53	1.791	1.062	0.975	0.553	a	0.470	0.652	56	1.672	0.507	0.987	0.738	b	0.627	0.876	31	1.315	−0.280	0.963	1.237	a	0.931	1.645

R^2: determination coefficient of linearized data regressions, F_{max0}: characteristic force of fracture (value at which 63.2% of the plates break), F_{max0} IC $_{95\%}$ ± : lower and upper limits of 95% confidence interval. Values sharing the same superscript in the same arm segment for the same variable did not differ significantly.

Table 6
Results of Weibull model applied to Young modulus (E).

Segment of the arm	Distal								Median								Proximal							
Nominal pH	n	m	C	R^2	E_0(GPa)		E_0 (GPa) $IC_{95\%}$ -	E_0 (GPa) $IC_{95\%}$ +	n	m	C	R^2	E_0(GPa)		E_0 (GPa) $IC_{95\%}$ -	E_0 (GPa) $IC_{95\%}$ +	n	m	C	R^2	E_0(GPa)		E_0 (GPa) $IC_{95\%}$ -	E_0 (GPa) $IC_{95\%}$ +
8.0	49	0.792	−2.003	0.918	12.54	a	8.56	18.36	41	0.985	−1.914	0.977	6.98	a	4.99	9.76	32	0.724	−0.781	0.924	2.94	a	1.75	4.94
7.4	56	0.809	−1.981	0.987	11.57	a	8.17	16.44	43	1.186	−1.947	0.927	5.16	a	3.93	6.78	29	0.750	−0.964	0.969	3.62	a	2.14	6.12
7.2	50	0.710	−1.312	0.981	6.35	a	4.16	9.69	54	0.878	−1.526	0.912	5.68	b	4.09	7.90	30	0.955	−1.420	0.882	4.42	a	2.93	6.68

R^2: determination coefficient of linearized data regressions, E_0: characteristic elasticity (value at which 63.2% of the plates break) E_0 IC $_{95\%}$ ± : lower and upper limits of 95% confidence interval. Values sharing the same superscript in the same arm segment for the same variable did not differ significantly.

Table 7
Nanoelasticity (Young modulus, E) and nanohardness (H) of distal adambulacral spines and ambulacral plates of *A. rubens*, according to the treatments (mean ± s.d., n = 5 individuals).

	pH_T	Young Modulus (GPa)			p ANOVA	Hardness (GPa)			p ANOVA
Plates	8.0	54.28	±	3.97	0.067	4.49	±	0.29	0.063
	7.4	59.14	±	7.17		4.92	±	0.59	
	7.2	54.34	±	13.17		4.12	±	0.64	
Spines	8	50.42	±	10.26	0.608	3.43	±	1.01	0.242
	7.4	53.43	±	7.36		3.32	±	0.70	
	7.2	42.62	±	6.35		2.57	±	0.69	

Table 8
mol% $MgCO_3$ in the cleaned skeleton of distal and proximal arm segments of *A. rubens* according to the treatments (m ± sd, *n* = 14).

Segment of the arm	pH	mol% $MgCO_3$			$P_{ANOVA\ pH}$	$P_{ANOVA\ segment}$	$P_{ANOVA\ pH*segment}$
Distal	8.0	7.28	±	1.13	0.909	**0.040**	0.437
	7.4	8.21	±	0.86			
	7.2	8.05	±	1.26			
Proximal	8.0	6.73	±	1.14			
	7.4	7.92	±	2.99			
	7.2	6.76	±	1.28			

Funding sources

This work was supported by Scientific Research Funds (FNRS grant n° J.0219.16 SOFTECHI).

Authors contributions

Concept/design, acquisition of data, data analysis/interpretation, drafting of the manuscript: S.D. Concept/design, drafting of the manuscript: Ph.D. Acquisition of data: Ph.P., L.M.; Acquisition of animals and acidification experiment: E.L., M.Y·H., M.S., F.M.

All authors contributed to revising the manuscript and approved the manuscript.

Acknowledgments

S. Di Giglio is a holder of a Belgian FRIA grant. P. Dubois is a Research Director of the National Fund for Scientific Research (FRS-FNRS; Belgium). M.Y.Hu is funded through the DFG Emmy Noether Programme HU2611/1-1. We would like to thank Professors I. Eeckhaut and P. Flammang and N. Puozzo for providing access to the SEM, S. De Kegel for her help with the preparation of resins for nanoindentation experiments and A. Fita-Codina for his participation in the improvement of the metal stand used for the three-point bending tests. We thank M. Leermakers and Ph. Claeys for providing access to the Milestone 1200 M microwave oven. The study was supported by FNRS grant n° J.0219.16 SOFTECHI. We thank Dr. Jason Hodin and two anonymous reviewers for their constructive suggestions.

Appendix A. Supplementary data

Supplementary data to this article can be found online at https://doi.org/10.1016/j.jembe.2020.151335.

References

Aizenberg, J., Hanson, J., Koetzle, T.F., Weiner, S., Addadi, L., 1997. Control of macromolecule distribution within synthetic and biogenic single calcite crystals. J. Am. Chem. Soc. 119, 881–886. https://doi.org/10.1021/ja9628821.

Andersson, A.J., MacKenzie, F.T., Lerman, A., 2005. Coastal Ocean and carbonate systems in the high CO_2 world of the anthropocene. Am. J. Sci. 305, 875–918. https://doi.org/10.2475/ajs.305.9.875.

Anger, K., Rogal, U., Schriever, G., Valentin, C., 1977. In-situ investigations on the echinoderm Asterias rubens as a predator of soft-bottom communities in the western Baltic Sea. Helgoländer Meeresun. 29, 439–459. https://doi.org/10.1007/BF01609982.

Appelhans, Y., Thomsen, J., Pansch, C., Melzner, F., Wahl, M., 2012. Sour times: seawater acidification effects on growth, feeding behaviour and acid–base status of *Asterias rubens* and *Carcinus maenas*. Mar. Ecol. Prog. Ser. 459, 85–98. https://doi.org/10.3354/meps09697.

Appelhans, Y.S., Thomsen, J., Opitz, S., Pansch, C., Melzner, F., Wahl, M., 2014. Juvenile Sea stars exposed to acidification decrease feeding and growth with no acclimation potential. Mar. Ecol. Prog. Ser. 509, 227–239. https://doi.org/10.3354/meps10884.

Asnaghi, V., Collard, M., Mangialajo, L., Gattuso, J.P., Dubois, P., 2019. Bottom-up effects on biomechanical properties of the skeletal plates of the sea urchin *Paracentrotus lividus* (Lamarck, 1816) in an acidified ocean scenario. Mar. Environ. Res. 144, 56–61. https://doi.org/10.1016/j.marenvres.2018.12.002.

Barnes, H., Powell, H.T., 1951. The growth-rate of juvenile *Asterias rubens* L. J. Mar. Biol. Assoc. United Kingdom 30, 381. https://doi.org/10.1017/S0025315400012844.

Ben Khadra, Y., Ferrario, C., Di Benedetto, C., Said, K., Bonasoro, F., Candia Carnevali, M.D., Sugni, M., 2015. Re-growth, morphogenesis, and differentiation during starfish arm regeneration. Wound Repair Regen. 23, 623–634. https://doi.org/10.1111/wrr.12336.

Blowes, L.M., Ergetová, M., Liu, Y., Davis, G.R., Terrill, N.J., Gupta, H.S., Elphick, M.R., 2017. Body wall structure in the starfish *Asterias rubens*. J. Anatomy 231, 325–341. https://doi.org/10.1111/joa.12646.

Bütikofer, L., Stawarczyk, B., Roos, M., 2015. Two regression methods for estimation of a two-parameter Weibull distribution for reliability of dental materials. Dent. Mater. 31, e33–e50. https://doi.org/10.1016/j.dental.2014.11.014.

Byrne, M., Fitzer, S., 2019. The Impact of Environmental Acidification on the Microstructure and Mechanical Integrity of Marine Invertebrate Skeletons 7, 1–21. https://doi.org/10.1093/conphys/coz062.

Caldeira, K., Wickett, M.E., 2003. Oceanography: anthropogenic carbon and ocean pH. Nature 425, 365. https://doi.org/10.1038/425365a.

Cao, L., Caldeira, K., 2008. Atmospheric CO_2 stabilization and ocean acidification. Geophys. Res. Lett. 35, 1–5. https://doi.org/10.1029/2008GL035072.

Chave, K.E., 1954. Aspects of the biogeochemistry of magnesium 1. Calcareous marine organisms. J. Geol. 62, 266–283. https://doi.org/10.1086/626162.

Collard, M., Dery, A., Dehairs, F., Dubois, P., 2014. Comparative biochemistry and physiology, Part A Euechinoidea and Cidaroidea respond differently to ocean acidi fi cation. Comp. Biochem. Physiol. A 174, 45–55. https://doi.org/10.1016/j.cbpa.2014.04.011.

Collard, M., Catarino, A.I., Bonnet, S., Flammang, P., Dubois, P., 2013. Effects of CO_2-induced ocean acidification on physiological and mechanical properties of the starfish *Asterias rubens*. Journal of Experimental Marine Biology and Ecology 446, 355–362. https://doi.org/10.1016/j.jembe.2013.06.003.

Collard, M., De Ridder, C., David, B., Dehairs, F., Dubois, P., 2015. Could the acid-base status of Antarctic Sea urchins indicate a better-than-expected resilience to near-future ocean acidification? Glob. Chang. Biol. 21, 605–617. https://doi.org/10.1111/gcb.12735.

Collard, M., Rastrick, S.P.S., Calosi, P., Demolder, Y., Dille, J., Findlay, H.S., Hall-spencer, J.M., Milazzo, M., Moulin, L., Widdicombe, S., Dehairs, F., Dubois, P., 2016. The impact of ocean acidification and warming on the skeletal mechanical properties of the sea urchin *Paracentrotus lividus* from laboratory and field observations. ICES J. 12. https://doi.org/10.1093/icesjms/fsv018.

Cyronak, T., Shulz, K.G., Jokiel, P.L., 2015. The omega myth, what really drives lower calcification rates in an acidifying ocean. ICES J. Mar. Sci. https://doi.org/10.1093/icesjms/fsv075. 10.1093/icesjms/fst176.

Dery, A., Collard, M., Dubois, P., 2017. Ocean acidification reduces spine mechanical strength in euechinoid but not in cidaroid sea urchins. Environ. Sci. Technol. 51, 3640–3648. https://doi.org/10.1021/acs.est.6b05138.

Doncaster, C.P., Davey, A.J.H., 2007. Analysis of Variance and Covariance: How to Choose and Construct Models for the Life Sciences. https://doi.org/10.1080/02664760902885203.

Eylers, J.P., 1976. Aspects of skeletal mechanics of the starfish *Asterias forbesii*. J. Morphol. 149, 353–368. https://doi.org/10.1093/icesjms/fsv018.

Fewkes, J.W., 1888. On the development of the calcareous plates of *Asterias*. Bull. Mus. Comp. Zool. 17.

Fietzek, P., Hiebenthal, C., 2017. Kiel Fjord pCO2 Datasets between 2015 (February) and 2016 (January) Measured Using a HydroC® pCO2 Sensor. https://doi.org/10.1594/PANGAEA.876548.

Flammang, P., 1996. Adhesion in echinoderms. Echinoderm. Stud. 5, 1–60.

Gattuso, J.-P., Hansson, L., 2009. Chapter 1: Ocean acidification: background and history. In: Ocean Acidification, pp. 1–20.

Gooding, R. a, Harley, C.D.G., Tang, E., 2009. Elevated water temperature and carbon dioxide concentration increase the growth of a keystone echinoderm. Proc. Natl. Acad. Sci. U. S. A. 106, 9316–9321. https://doi.org/10.1073/pnas.0811143106.

Govindaraju, 1994. Compilation of working values and sample description for 383 geostandards. Geostand. Newslett. 18, 1.

Guillou, M., Joly-Turquin, G., Leyzour, S., Pernet, P., Dubois, P., 2012. Factors controlling juvenile growth and population structure of the starfish *Asterias rubens* in intertidal habitats: field and experimental approaches. J. Mar. Biol. Assoc. United Kingdom 92, 367–378. https://doi.org/10.1017/S0025315411001020.

Hennebert, E., Haesaerts, D., Dubois, P., Flammang, P., 2010. Evaluation of the different forces brought into play during tube foot activities in sea stars. J. Exp. Biol. 213, 1162–1174. https://doi.org/10.1242/jeb.037903.

Hiebenthal, C., Fietzek, P., Thomsen, J., Saderne, V., Melzner, F., 2016. Kiel fjord pCO_2 datasets between 2012 (July) and 2015 (January) measured using a HydroC® pCO2 sensor. Kiel; PANGAEA. https://doi.org/10.1594/PANGAEA.859407.

Holtmann, W.C., Stumpp, M., Gutowska, M.A., Syré, S., Himmerkus, N., Melzner, F., Bleich, M., 2013. Maintenance of coelomic fluid pH in sea urchins exposed to elevated CO_2: the role of body cavity epithelia and stereom dissolution. Marine Biology 160 (10), 2631–2645. https://doi.org/10.1007/s00227-013-2257-x.

Hotchkiss, F.H.C., 2012. Growth zones and extraxial-axial skeletal homologies in Asteroidea (Echinodermata). Proc. Biol. Soc. Wash. 125, 106–121. https://doi.org/10.2988/11-37.1.

Hu, M.Y., Lein, E., Bleich, M., Melzner, F., Stumpp, M., 2018. Trans-life cycle acclimation to experimental ocean acidification affects gastric pH homeostasis and larval recruitment in the sea star *Asterias rubens*. Acta Physiol., e13075. https://doi.org/10.1111/apha.13075.

Hu, M.Y., Yan, J.-J., Petersen, I., Himmerkus, N., Bleich, M., Stumpp, M., 2018b. A SLC4 family bicarbonate transporter is critical for intracellular pH regulation and biomineralization in sea urchin embryos. Elife 7, e36600. https://doi.org/10.7554/eLife.36600.

Hughes, S.J.M., Ruhl, H. a, Hawkins, L.E., Hauton, C., Boorman, B., Billett, D.S.M., 2011. Deep-sea echinoderm oxygen consumption rates and an interclass comparison of metabolic rates in Asteroidea, Crinoidea, Echinoidea, Holothuroidea and Ophiuroidea. J. Exp. Biol. 214, 2512–2521. https://doi.org/10.1242/jeb.055954.

IPCC, 2014. Intergovernmental Panel on Climate Change. Climate Change 2014 Synthesis Report.

Kamya, P.Z., Byrne, M., Graba-Landry, A., Dworjanyn, S.A., 2016. Near-Future Ocean acidification enhances the feeding rate and development of the herbivorous juveniles of the crown-of-thorns starfish, *Acanthaster planci*. Coral Reefs 35, 1241–1251. https://doi.org/10.1007/s00338-016-1480-6.

Kamya, P.Z., Byrne, M., Mos, B., Hall, L., Dworjanyn, S.A., 2017. Indirect effects of ocean acidification drive feeding and growth of juvenile crownof- thorns starfish, *Acanthaster planci*. Proc. R. Soc. B Biol. Sci. 284. https://doi.org/10.1098/rspb.2017.0778.

Keppel, E.A., Scrosati, R.A., Courtenay, S.C., 2015. Interactive effects of ocean acidification and warming on subtidal mussels and sea stars from Atlantic Canada. Mar. Biol. Res. 11, 337–348. https://doi.org/10.1080/17451000.2014.932914.

Kroeker, K.J., Kordas, R.L., Crim, R., Hendriks, I.E., Ramajo, L., Singh, G.S., Duarte, C.M., Gattuso, J.P., 2013. Impacts of ocean acidification on marine organisms: quantifying sensitivities and interaction with warming. Glob. Chang. Biol. 19, 1884–1896. https://doi.org/10.1111/gcb.12179.

Lebrato, M., Andersson, A.J., Ries, J.B., Aronson, R.B., Lamare, M.D., Koeve, W., Oschlies, A., Iglesias-Rodriguez, M.D., Thatje, S., Amsler, M., Vos, S.C., Jones, D.O.B., Ruhl, H.A., Gates, A.R., McClintock, J.B., 2016. Benthic marine calcifiers coexist with $CaCO_3$-undersaturated seawater worldwide. Glob. Biogeochem. Cycles 30, 1038–1053. https://doi.org/10.1002/2015GB005260.

Leung, B.T.W., Tsoi, J.K.H., Matinlinna, J.P., Pow, E.H.N., 2015. Comparison of mechanical properties of three machinable ceramics with an experimental fluorophlogopite glass ceramic. J. Prosthet. Dent. 114, 440–446. https://doi.org/10.1016/j.prosdent.2015.02.024.

Lin, A.Y.M., Meyers, M.A., Vecchio, K.S., 2006. Mechanical properties and structure of *Strombus gigas*, *Tridacna gigas*, and *Haliotis rufescens* sea shells: a comparative study. Mater. Sci. Eng. C 26, 1380–1389. https://doi.org/10.1016/j.msec.2005.08.016.

Mcclintock, J.B., Robnett, T.J., 1986. Size selective predation by the asteroid pisaster ochraceus on the bivalve *Mytilus californianus*: a cost-benefit analysis. Mar. Ecol. 7, 321–332. https://doi.org/10.1111/j.1439-0485.1986.tb00167.x.

Melzner, F., Gutowska, M.A., Langenbuch, M., Dupont, S., Lucassen, M., Thorndyke, M.C., Bleich, M., Pörtner, H.-O., 2009. Physiological basis for high CO_2 tolerance in marine ectothermic animals: pre-adaptation through lifestyle and ontogeny? Biogeosci. Discuss. https://doi.org/10.5194/bgd-6-4693-2009.

Melzner, F., Thomsen, J., Koeve, W., Oschlies, A., Gutowska, M., Bange, H.W., Hansen, H.P., Körtzinger, A., 2013. Future Ocean acidification will be amplified by hypoxia in coastal habitats. Mar. Biol. 160, 1875–1888. https://doi.org/10.1007/s00227-012-1954-1.

Morse, J.W., Andersson, A.J., Mackenzie, F.T., 2006. Initial responses of carbonate-rich shelf sediments to rising atmospheric pCO_2 and "ocean acidification": role of high Mg-calcites. Geochim. Cosmochim. Acta 70, 5814–5830. https://doi.org/10.1016/j.gca.2006.08.017.

Moulin, L., Grosjean, P., Leblud, J., Batigny, A., Collard, M., Dubois, P., 2015. Long-term mesocosms study of the effects of ocean acidification on growth and physiology of the sea urchin *Echinometra mathaei*. Mar. Environ. Res. 103, 103–114. https://doi.org/10.1016/j.marenvres.2014.11.009.

Moureaux, C., Simon, J., Mannaerts, G., Catarino, A.I., Pernet, P., Dubois, P., 2011. Effects of field contamination by metals (Cd, Cu, Pb, Zn) on biometry and mechanics of echinoderm ossicles. Aquat. Toxicol. 105, 698–707. https://doi.org/10.1016/j.aquatox.2011.09.007.

Navarrete, S.A., Menge, B.A., 1996. Keystone predation and interaction strength : interactive effects of predators on their main prey. Ecol. Monogr. 66, 409–429.

Naviaux, J.D., Subhas, A.V., Rollins, N.E., Dong, S., Berelson, W.M., Adkins, J.F., 2019. Temperature dependence of calcite dissolution kinetics in seawater. Geochim. Cosmochim. Acta 246, 363–384. https://doi.org/10.1016/j.gca.2018.11.037.

Norberg, J., Tedengren, M., 1995. Attack behaviour and predatory success of *Asterias rubens* L. related to differences in size and morphology of the prey mussel Mytilus edulis L. J. Exp. Mar. Biol. Ecol. 186, 207–220. https://doi.org/10.1016/0022-0981(94)00158-A.

Oliver, G.M., Pharr, W.C., 1992. Measurement of thin film mechanical properties using nanoindentation. MRS Bull. 17, 28–33.

Orr, J.C., Fabry, V.J., Aumont, O., Bopp, L., Doney, S.C., Feely, R.M., Gnanadesikan, A., Gruber, N., Ishida, A., Key, R.M., Lindsay, K., Maier-reimer, E., Matear, R., Monfray, P., Mouchet, a, Najjar, R.G., Plattner, G.K., Rodgers, K.B., Sabine, C.L., Sarmiento, J.L., Schlitzer, R., Slater, R.D., Totterdell, I.J., Weirig, M.F., Yamanaka, Y., Yool, a, Matear, R., 2005. Anthropogenic decline in high-latitude ocean carbonate by 2100. Nature 437, 681–686.

Paine, V.L., 1926. Adhesion of the tube feet in starfishes. J. Exp. Zool. 45, 361–366. https://doi.org/10.1002/jez.1400450115.

Paine, R.T., 1974. Intertidal community structure: experimental studies on the relationship between a dominant competitor and its principal predator. Oecologia 15, 93–120.

Politi, Y., Arad, T., Klein, E., Weiner, S., Addadi, L., 2004. Sea urchin spine Calcite Forms via a transient amorphous calcium carbonate phase. Science 306, 1161–1164. https://doi.org/10.1126/science.1102289.

Presser, V., Gerlach, K., Vohrer, A., Nickel, K.G., Dreher, W.F., 2010. Determination of the elastic modulus of highly porous samples by nanoindentation: a case study on sea urchin spines. J. Mater. Sci. 45, 2408–2418. https://doi.org/10.1007/s10853-010-4208-y.

Reusch, T.B.H., Dierking, J., Andersson, H.C., Bonsdorff, E., Carstensen, J., Casini, M., Czajkowski, M., Hasler, B., Hinsby, K., Hyytiäinen, K., 2018. The Baltic Sea as a time machine for the future coastal ocean. Sci. Adv. 4. https://doi.org/10.1126/sciadv.aar8195.

Saier, B., 2001. Direct and indirect effects of seastars *Asterias rubens* on mussel beds (*Mytilus edulis)* in the Wadden Sea. Hydrobiologia 440, 119–128. https://doi.org/10.1023/A:1004142306396.

Schram, J.B., McClintock, J.B., Angus, R.A., Lawrence, J.M., 2011. Regenerative capacity and biochemical composition of the sea star *Luidia clathrata* (Say) (Echinodermata: Asteroidea) under conditions of near-future ocean acidification. J. Exp. Mar. Biol. Ecol. 407, 266–274. https://doi.org/10.1016/j.jembe.2011.06.024.

Stumpp, M., Trübenbach, K., Brennecke, D., Hu, M.Y., Melzner, F., 2012. Resource allocation and extracellular acid-base status in the sea urchin *Strongylocentrotus droebachiensis* in response to CO_2 induced seawater acidification. Aquat. Toxicol. 110–111, 194–207. https://doi.org/10.1016/j.aquatox.2011.12.020.

Suwa, R., Hatta, M., Ichikawa, K., 2014. Proton-transfer reaction dynamics and energetics in calcification and decalcification. Chem. - A Eur. J. 1–7. https://doi.org/10.1002/chem.201402210.

Thomsen, J., Gutowska, M.A., Saphörster, J., Heinemann, A., Trübenbach, K., Fietzke, J., Hiebenthal, C., Eisenhauer, A., Körtzinger, A., Wahl, M., Melzner, F., 2010. Calcifying invertebrates succeed in a naturally CO_2-rich coastal habitat but are threatened by high levels of future acidification. Biogeosciences 7, 3879–3891. https://doi.org/10.5194/bg-7-3879-2010.

Thomsen, J., Casties, I., Pansch, C., Körtzinger, A., Melzner, F., 2013. Food availability outweighs ocean acidification effects in juvenile *Mytilus edulis* : laboratory and field experiments. Glob. Chang. Biol. 19, 1017–1027. https://doi.org/10.1111/gcb.12109.

Thomsen, J., Stapp, L.S., Haynert, K., Schade, H., Danelli, M., Lannig, G., Wegner, K.M., Melzner, F., 2017. Naturally acidified habitat selects for ocean acidification–tolerant mussels. Sci. Adv. 3. https://doi.org/10.1126/sciadv.1602411.

Uthicke, S., Schaffelke, B., Byrne, M., 2009. A boom–bust phylum? Ecological and evolutionary consequences of density variations in echinoderms. Ecol. Monogr. 79, 3–24.

Weber, J.N., 1969. The incorporation of magnesium into the skeletal calcites of echinoderms. Am. J. Sci. https://doi.org/10.2475/ajs.267.5.537.

Wittmann, A.C., Pörtner, H.O., 2013. Sensitivities of extant animal taxa to ocean acidification. Nat. Clim. Chang. 3, 995–1001. https://doi.org/10.1038/nclimate1982.

Zafiriou, O., Whittle, K.J., Blumer, M., 1972. Response of *Asterias vulgaris* to bivalves and bivalve tissue extracts. Mar. Biol. 13, 137–145. https://doi.org/10.1007/BF00366564.